ADVANCED SCIENCE NEWS
www.advancedsciencenews.com

NANO MICRO small

GaP/GaNP Heterojunctions for Efficient Solar-Driven Water Oxidation

Alireza Kargar, Supanee Sukrittanon, Chang Zhou, Yun Goo Ro, Xiaoqing Pan, Shadi A. Dayeh, Charles W. Tu, and Sungho Jin**

The growth and characterization of an n-GaP/i-GaNP/p$^+$-GaP thin film heterojunction synthesized using a gas-source molecular beam epitaxy (MBE) method, and its application for efficient solar-driven water oxidation is reported. The TiO_2/Ni passivated n-GaP/i-GaNP/p$^+$-GaP thin film heterojunction provides much higher photoanodic performance in 1 M KOH solution than the TiO_2/Ni-coated n-GaP substrate, leading to much lower onset potential and much higher photocurrent. There is a significant photoanodic potential shift of 764 mV at a photocurrent of 0.34 mA cm^{-2}, leading to an onset potential of ≈0.4 V versus reversible hydrogen electrode (RHE) at 0.34 mA cm^{-2} for the heterojunction. The photocurrent at the water oxidation potential (1.23 V vs RHE) is 1.46 and 7.26 mA cm^{-2} for the coated n-GaP and n-GaP/i-GaNP/p$^+$-GaP photoanodes, respectively. The passivated heterojunction offers a maximum applied bias photon-to-current efficiency (ABPE) of 1.9% while the ABPE of the coated n-GaP sample is almost zero. Furthermore, the coated n-GaP/i-GaNP/p$^+$-GaP heterojunction photoanode provides a broad absorption spectrum up to ≈620 nm with incident photon-to-current efficiencies (IPCEs) of over 40% from ≈400 to ≈560 nm. The high low-bias performance and broad absorption of the wide-bandgap GaP/GaNP heterojunctions render them as a promising photoanode material for tandem photoelectrochemical (PEC) cells to carry out overall solar water splitting.

Dr. A. Kargar, Y. G. Ro, Prof. S. A. Dayeh, Prof. C. W. Tu
Department of Electrical and Computer Engineering
University of California-San Diego
La Jolla, CA 92093, USA
E-mail: ctu@ece.ucsd.edu

Dr. S. Sukrittanon, Prof. S. A. Dayeh, Prof. C. W. Tu, Prof. S. Jin
Materials Science and Engineering Program
University of California-San Diego
La Jolla, CA 92093, USA
E-mail: jin@ucsd.edu

C. Zhou
School of Materials Science and Engineering
Harbin Institute of Technology
Harbin, Heilongjiang 150001, P. R. China

C. Zhou, Prof. X. Pan
Department of Materials Science and Engineering
University of Michigan
Ann Arbor, MI 48109, USA

Prof. X. Pan
Department of Chemical Engineering
and Materials Science
University of California-Irvine
Irvine, CA 92697, USA

Prof. X. Pan
Department of Physics and Astronomy
University of California-Irvine
Irvine, CA 92697, USA

Prof. S. Jin
Department of Mechanical and Aerospace Engineering
University of California-San Diego
La Jolla, CA 92093, USA

DOI: 10.1002/smll.201603574

 © 2017 Wiley-VCH Verlag GmbH & Co. KGaA, Weinheim

Hydrogen, a clean and sustainable energy carrier, is considered as a promising approach to meet the growing energy demands.[1–3] A promising method for the production of hydrogen is solar-driven water splitting using PEC cells,[4–9] which can offer high solar-to-hydrogen (STH) efficiencies of over 28%.[10] A key step in the PEC cells is solar-driven oxidation of water to oxygen. In fact, the solar water oxidation is more challenging than the solar water reduction due to the nature of its reaction and the fact that it requires four electron transfer steps compared to two electron transfer steps needed for the water reduction. The low STH efficiency of the reported tandem PEC cells for overall solar water splitting is mainly due to inefficient photoanodes, which are unable to offer high solar water oxidation performance at low biasing potentials with a low onset potential and a high photocurrent.[11–15] As such, developing photoanodes with high performance at low biasing potentials is necessary to make efficient tandem PEC cells for high-efficiency solar hydrogen production.

Protected III–V photoanode materials have shown promising performances for the solar water oxidation owing to their unique properties.[9,16–19] In particular, n-GaP with a bandgap of 2.26 eV can be a promising photoanode material.[16,20,21] GaP has a proper bandgap to provide a high photovoltage, a relatively suitable energy band alignment for the solar water oxidation,[1] and a high carrier mobility.[22,23] Additionally, GaP is a mature semiconductor material widely used in light emitting diodes.[24,25] P-GaP is considered as one of the most promising photocathode materials for the solar-driven water reduction due to its high conduction band edge and its large photovoltage.[26–32] However, n-GaP with an indirect bandgap and a low absorption coefficient (absorption coefficient in the range of 10^2–10^3 cm^{-1} above the band edge)[33] cannot provide a high-efficiency solar water oxidation performance.[16] A direct bandgap semiconductor with a tunable bandgap and an absorption coefficient of around 10^4 cm^{-1} above the band edge can be made by adding a small amount of N to GaP to result in gallium nitride phosphide, GaNP.[34,35] Moreover, formation of a GaP p–n junction within the photoanode material can increase the photovoltage assisting to further improve the solar conversion efficiency.[36]

Herein, we report a novel GaP photoanode material; n-GaP/i-GaNP/p^+-GaP thin film heterojunction, consisting of direct bandgap GaNP with a smaller bandgap on the top of GaP forming a GaP/GaNP heterojunction and a buried top junction, fabricated using a gas-source MBE technique for efficient solar water oxidation. The morphology and structure of the n-GaP/i-GaNP/p^+-GaP heterojunction is characterized in detail using scanning and transmission electron microscopies. The TiO_2/Ni passivated n-GaP/i-GaNP/p^+-GaP heterojunction provides much higher photoanodic performance in 1 M KOH electrolyte than the TiO_2/Ni-coated n-GaP substrate, resulting in much lower onset potential and much higher photocurrent. The coated heterojunction provides a maximum applied ABPE of 1.9% while the passivated n-GaP ABPE is nearly zero. The coated n-GaP/i-GaNP/p^+-GaP heterojunction photoanode also offers a wide absorption spectrum. The mechanism of performance improvement is studied using optical absorption property and energy band diagram.

Figure 1a shows a schematic representation of the n-GaP/i-GaNP/p^+-GaP thin film heterojunction substrate in which an i-GaNP layer with a thickness of 800 nm and a top p^+-GaP layer with a thickness of 100 nm were grown on the n-GaP planar substrate (see the Experimental Section for details). Scanning electron microscopy (SEM) image (Figure 1b) exhibits the uniform growth of i-GaNP layer on the n-GaP substrate. The boundary between the n-GaP substrate and i-GaNP layer can clearly be realized from the contrast change shown in Figure 1c.

Transmission electron microscopy (TEM) images of the n-GaP/i-GaNP/p^+-GaP thin film substrate is shown in Figure 1d–k. The low-magnification cross-sectional TEM images (Figure 1d,e) exhibit the stacking of three layers in which the boundary between n-GaP and i-GaNP can clearly be realized (Figure 1d) as also shown in Figure 1c. The interface between n-GaP and i-GaNP is a defective interface (as can be seen from the clearly visible defect contrast at the interface in Figure 1d) with misfit defects leading to misfit dislocation.[34] The boundary between i-GaNP and p^+-GaP is hard to clearly observe (Figure 1e) possibly due to a very small lattice mismatch, which will be discussed in the following. The grown i-GaNP and p^+-GaP layers are single crystalline as shown in high-resolution TEM (HRTEM) images (Figure 1f,g) revealing formation of epitaxial layers. The single crystallinity further confirms with the fast Fourier transform (FFT) pattern (insets of Figure 1f,g), which also indicates a growth direction of [001]. There is a very small difference in the calculated lattice spacing of i-GaNP and p^+-GaP layers (0.312 vs 0.314 nm (Figure 1f,g) indicating a minimal lattice mismatch. The minimal lattice mismatch is due to the incorporation of a small amount of N into the GaP ([N] ≈ 1.8%[34]). The crystal structure, however, remains unchanged with such a small incorporation of N (see Figure S1 in the Supporting Information). The energy dispersive X-ray spectroscopy (EDS) spectrum (Figure 1h) confirms the formation of GaNP with a small amount of N. The surface structure of the n-GaP/i-GaNP/p^+-GaP thin film substrate is rough exhibiting a textured surface with a texture size of several nanometers (Figure 1i–k). The facets of such a rough surface are identified and shown in Figure S2 (Supporting Information). The reason for the formation of rough surface is not totally clear at this point though it may be due to postgrowth heating or introduction of dopants. High temperature of the growth may be another reason for the formation of GaP rough surface.[37]

Figure 2 exhibits the optical absorption spectra of the n-GaP and n-GaP/i-GaNP/p^+-GaP thin film substrates in which the n-GaP/i-GaNP/p^+-GaP heterojunction shows higher absorption than the n-GaP. For wavelengths below ≈525 nm, the difference in the optical absorption is not that significant (Figure 2 inset) while for higher wavelengths, the difference is much higher. For wavelengths below ≈525 nm, the higher absorption may be due to the textured surface of the n-GaP/i-GaNP/p^+-GaP substrate (Figure 1i–k), and for higher wavelengths, it can be mostly because of the GaNP layer with a smaller bandgap (≈2.05 eV[34]) absorbing a broader spectrum (see **Figure 3**e).

© 2017 Wiley-VCH Verlag GmbH & Co. KGaA, Weinheim

NANO MICRO small

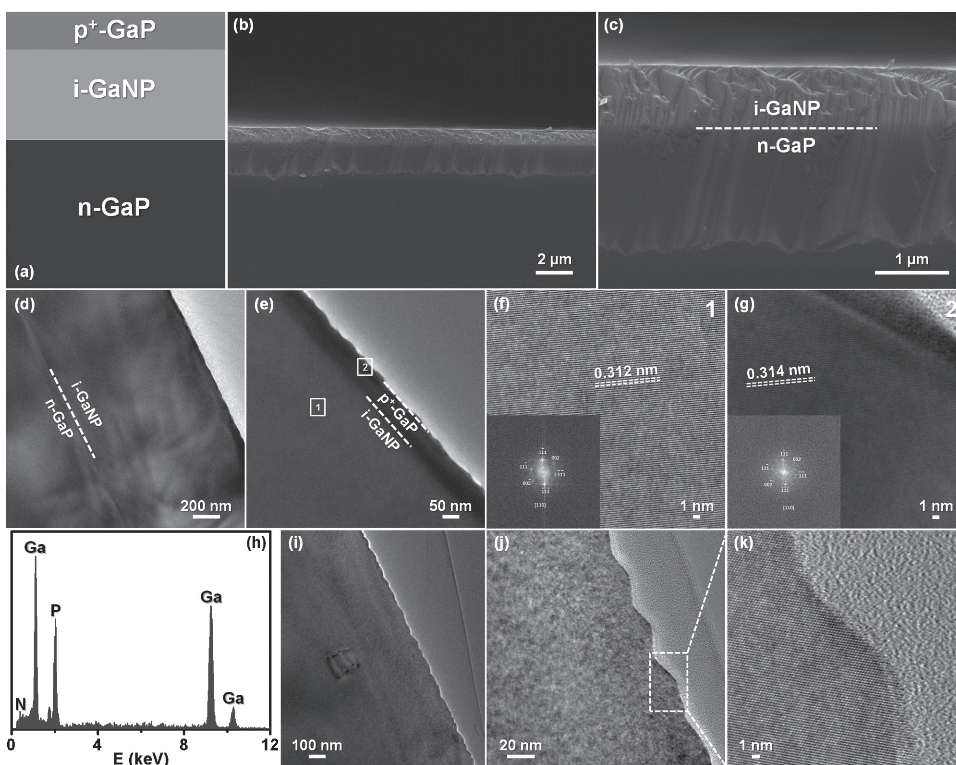

Figure 1. a) Schematic representation and b,c) low- and high-magnification cross-sectional SEM images of n-GaP/i-GaNP/p+-GaP thin film substrate. d) Low-magnification and e) higher-magnification cross-sectional TEM images of n-GaP/i-GaNP/p+-GaP thin film substrate. HRTEM image of f) i-GaNP layer (marked region with "1" in panel (e)) and g) p+-GaP layer (labeled area with "2" in panel (e)). Insets are the corresponding FFT patterns. h) EDS spectrum of i-GaNP layer. i) Low-magnification TEM, j) high-magnification TEM, and k) HRTEM images of surface structure of n-GaP/i-GaNP/p+-GaP thin film substrate.

The n-GaP/i-GaNP/p+-GaP heterojunction sample is not stable during the PEC operation. Its surface was then passivated with a thin atomic layer-deposited TiO_2 layer accompanied with a Ni nanoparticle cocatalyst coating (see the Experimental Section for details). The PEC performance (linear sweep voltammetry (LSV) measurement) of the TiO_2/Ni-coated n-GaP and n-GaP/i-GaNP/p+-GaP photoanodes in 1 M KOH solution is shown in Figure 3a (see Figure S3 in the Supporting Information for cyclic voltammetry (CV) measurement) in which the n-GaP/i-GaNP/p+-GaP thin film heterojunction exhibits much higher photoanodic performance than the n-GaP substrate resulting in a much lower onset potential and a much higher photocurrent. There is a significant potential shift of 764 mV at a photocurrent of 0.34 mA cm^{-2}. The onset potential of the heterojunction is ≈0.4 V versus RHE at the 0.34 mA cm^{-2} photocurrent. The photocurrent at 1.23 V versus RHE (equilibrium potential for the water oxidation; the dotted line in Figure 3a) is 1.46 and 7.26 mA cm^{-2} for the TiO_2/Ni-coated n-GaP and n-GaP/i-GaNP/p+-GaP photoanodes, respectively. The saturation photocurrent of the n-GaP/i-GaNP/p+-GaP sample is over one and a half times larger than that of the n-GaP sample. The dark current of both samples is around zero. The enhanced photoanodic performance of the n-GaP/i-GaNP/p+-GaP heterojunction is due to (i) broader absorption spectrum (see Figure 3e), (ii) enhanced charge separation and collection (see Figure 3b), (iii) increased reaction surface area coming from the textured surface discussed earlier, and (iv) improved optical absorption (as shown in Figure 2). As shown in the energy band diagram (Figure 3b), the i-GaNP layer forms a junction with the n-GaP substrate and there is a junction between the i-GaNP and p+-GaP layers. Due to a very low doping of the i-GaNP layer (around 10^{15} cm^{-3}), the depletion layer extends across its whole width. Although there is

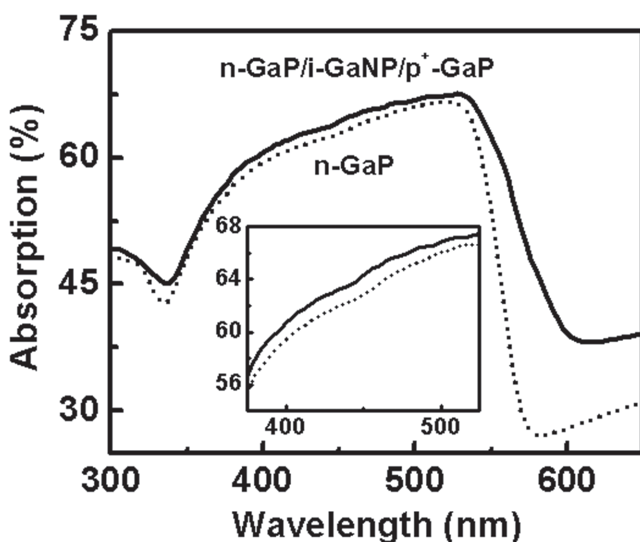

Figure 2. Optical absorption spectra of n-GaP and n-GaP/i-GaNP/p+-GaP thin film heterojunction substrates. Inset shows the zoomed-in absorption spectrum from 375 to 525 nm.

© 2017 Wiley-VCH Verlag GmbH & Co. KGaA, Weinheim

ADVANCED SCIENCE NEWS
www.advancedsciencenews.com

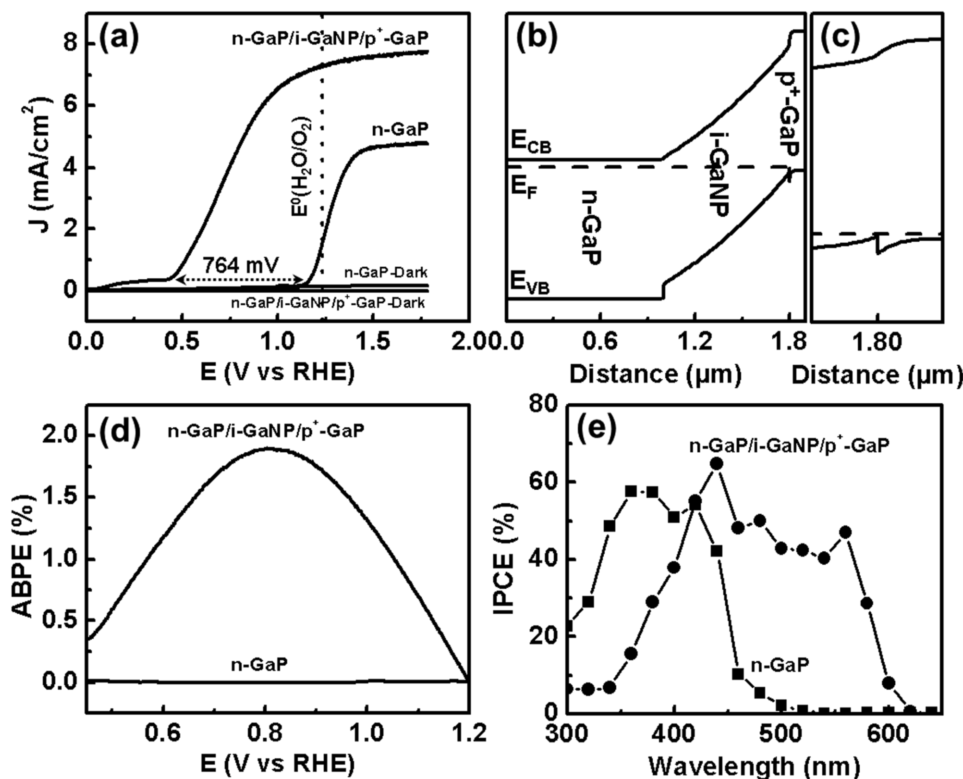

Figure 3. a) Linear sweep voltammetry (LSV) measurement at dark and under illumination of the TiO_2/Ni-coated n-GaP and n-GaP/i-GaNP/p^+-GaP thin film heterojunction substrates collected at a scan rate of 10 mV s^{-1} in 1 M KOH solution. b) Approximate energy band diagram of the n-GaP/i-GaNP/p^+-GaP heterojunction at equilibrium condition and at dark, which was simulated using SCAPS (version 3.1.02) numerical simulation software. c) Zoomed-in energy band diagram around i-GaNP and p^+-GaP junction. d) Applied bias photon-to-current efficiency (ABPE) of the corresponding samples in panel (a). e) Incident photon-to-current efficiency (IPCE) of the TiO_2/Ni-coated n-GaP and n-GaP/i-GaNP/p^+-GaP thin film heterojunction substrates at 1.4 V versus RHE recorded in 1 M KOH electrolyte.

a very small barrier for the holes in the i-GaNP/p^+-GaP junction (Figure 3c), the holes can thermionically be emitted and eventually transport into the electrolyte. As a result of the two junctions, the charge separation significantly improves. The separated charges then collect efficiently through the grown thin i-GaNP and p^+-GaP layers. The energy band diagram of the TiO_2-coated n-GaP and n-GaP/i-GaNP/p^+-GaP substrates is shown in Figure S4 (Supporting Information), highlighting the significant effect of the heterojunction in the enhanced charge separation and collection compared to that of the bare n-GaP. Low-bias performance (onset potential and photocurrent at low biasing potentials) of the n-GaP/i-GaNP/p^+-GaP heterojunction can further be improved by using a nanostructure morphology such as nanodome array.[38] The TiO_2/Ni-coated n-GaP/i-GaNP/p^+-GaP sample offers a maximum ABPE of 1.9% while the ABPE of the TiO_2/Ni-coated n-GaP sample is almost zero (Figure 3d).

The incident photon-to-current efficiency of the TiO_2/Ni-coated n-GaP and n-GaP/i-GaNP/p^+-GaP samples at 1.4 V versus RHE is shown in Figure 3e. The n-GaP/i-GaNP/p^+-GaP heterojunction provides a broader spectrum up to around 620 nm while the n-GaP substrate only covers up to around 520 nm. The wider spectrum is due to the i-GaNP layer with a smaller bandgap (≈2.05 eV). The n-GaP/i-GaNP/p^+-GaP heterojunction offers efficiencies of over 40% from around 400 nm to around 560 nm, while the n-GaP substrate provides comparable efficiencies from about 340 nm to around 440 nm. The high efficiencies of both samples are comparable confirming the small optical absorption improvement of the n-GaP/i-GaNP/p^+-GaP heterojunction (Figure 2).

In conclusion, the growth and characterization of the n-GaP/i-GaNP/p^+-GaP thin film heterojunction fabricated using the gas-source MBE, and its application for efficient solar-driven water oxidation is demonstrated. The epitaxially grown i-GaNP and p^+-GaP layers were single crystalline with a minimal lattice mismatch. The TiO_2/Ni-passivated n-GaP/i-GaNP/p^+-GaP heterojunction photoanode provided much higher PEC performance than the TiO_2/Ni-coated n-GaP substrate in 1 M KOH electrolyte, resulting in a significant potential shift of 764 mV at a photocurrent of 0.34 mA cm^{-2} (onset potential of ≈0.4 V vs RHE at 0.34 mA cm^{-2} for the heterojunction) and a high photocurrent of 7.26 mA cm^{-2} at 1.23 V versus RHE. The passivated heterojunction offers a maximum ABPE of 1.9%. Moreover, the coated n-GaP/i-GaNP/p^+-GaP photoanode offered a wide absorption spectrum up to ≈620 nm with the IPCEs of over 40% from ≈400 to ≈560 nm. The high low-bias performance and broad absorption of the coated wide-bandgap GaP/GaNP heterojunctions reveal their promising application for the tandem PEC cells to handle overall solar-driven water splitting in an alkaline electrolyte.

 © 2017 Wiley-VCH Verlag GmbH & Co. KGaA, Weinheim

Experimental Section

Fabrication of TiO_2/Ni-Coated n-GaP and n-GaP/i-GaNP/p$^+$-GaP Samples: All the samples reported in this work were grown on n-type (6×10^{17} cm^{-3}) GaP (001) substrate using a Varian Gen-II MBE system modified to handle gas sources. Thermally cracked PH_3 at 1000 °C and radio frequency N plasma excited at 13.56 MHz were used as P and N sources, respectively. Solid elemental Ga from an effusion cell was used to generate a Ga beam. Prior to the growth, the native oxide was desorbed under P_2 overpressure at 600 °C. The substrate temperature was then decreased to 570 °C to grow an 800 nm i-GaNP layer. A substrate temperature of 570 °C was chosen because it is in the optimal growth temperature range to minimize N-related defects before phase separation in dilute nitride. The following layer was 100 nm p$^+$-GaP (2×10^{18} cm^{-3}) using B as the dopant. All the layers were grown at a rate of 1 µm h^{-1} with a V/III incorporation ratio of ≈2.5, calibrated by Ga-induced reflection high energy electron diffraction intensity oscillation. The substrate was rotated at 5 rpm during the growth to ensure uniformity.

Bare n-GaP substrates were dipped into aqueous HCl solution (50% v/v) for 30 s, rinsed with deionized (DI) water, dried with N_2 gas, and transferred to atomic layer deposition (ALD) chamber (Beneq TFS 200 system) along with the n-GaP/i-GaNP/p$^+$-GaP substrates. Note that no cleaning was performed for the n-GaP/i-GaNP/p$^+$-GaP substrates right before the ALD deposition. A thin TiO_2 layer was then deposited on the substrates using ALD in thermal mode (thermal ALD) at a temperature of 300 °C. The number of cycles was 440 giving a thickness of ≈20 nm based on a growth rate of 0.454 Å per cycle on planar Si substrate. Note that the applied ALD TiO_2 coating is not the best developed ALD TiO_2 coating for the long-term stability and better coating has been reported elsewhere.[16] E-beam evaporation was finally used to deposit nominally 2 nm Ni on the TiO_2-coated substrates. Samples were then stored before any characterization.

Characterization: Sample morphology was examined using an ultrahigh-resolution scanning electron microscopy (FEI XL30-SFEG) working at an accelerating voltage of 15 kV. A high resolution transmission electron microscopy (JEOL JEM3011, HRTEM) operated at 300 kV was employed for the atomic-scale structural analyses. EDS was carried out to obtain the elemental information. Cross-sectional thin film specimens for the TEM and HRTEM imagings were prepared by mechanical polishing. Thin films were first glued to the sacrificial silicon with M-Bond 610 (Vishay Precision Group). Then, a single cut piece was placed on a wedge-polishing tool (T-tools, Precision TEM, Inc.), thinned, and fine-polished against diamond lapping papers (Southbay Technology, Inc.) of varying grit sizes before being glued with a molybdenum ring (Structure Probe, Inc.) with M-Bond 610 epoxy. The polished cross-sectional pieces were then ion-milled under Ar gas for polishing using a precision ion polishing system (Gatan model 695). The ion milling stops as the hole formed in silicon upon fine thinning reaches the film side.

Optical absorption measurements were achieved using a 150 mm integrating sphere connected to a LAMBDA 1050 UV–vis–NIR spectrophotometer. The absorption (A) was calculated using $A(\%) = 100 - R - T(\%)$, in which R is reflectance and T is transmittance. Energy band diagram was simulated using SCAPS (version 3.1.02) numerical simulation software. The considered thickness of the n-GaP, i-GaNP, and p$^+$-GaP layers were 1 µm, 800 nm, and 100 nm, respectively. The doping concentration of the n-GaP, i-GaNP, and p$^+$-GaP layers were considered as 10^{17}, 10^{15}, and 10^{18} cm^{-3}, respectively. The bandgap of n-GaP, i-GaNP, and p$^+$-GaP layers were considered as 2.26, 2.05, and 2.26 eV, respectively.[34]

Photoelectrochemical and IPCE Measurements: Ohmic contact was made to the GaP backside by scratching the backside with a diamond tip scribe, soldering indium on the back, annealing the sample at 400 °C for 10 min under forming gas, and finally attaching a coated Cu wire to the annealed contact with another indium soldering. The backside and edges of sample were then sealed using a Hysol 615 epoxy. Current density measurements were carried out in an aqueous solution of 1 M KOH (Fisher Chemical, 88.5%) at pH = 13.7 (DI water resistivity; 18.2 MΩcm) with a three-electrode configuration, including sample as working electrode, Pt gauze as counter electrode, and Hg/HgO (1 M NaOH) or Ag/AgCl (1 M KCl) as reference electrode (RE). A light power intensity of 100 mW cm^{-2} was adjusted at the sample position using a solar simulator (Newport 66905) with a xenon lamp equipped with the 1.5 AM filter. The current density measurements were collected using a potentiostat (Digi-Ivy, DY2300). A scan rate of 10 mV s^{-1} was employed for the LSV and CV measurements. During the measurements, a mild agitation was used and the electrolyte was constantly purged with a small flow of N_2 gas. The electrolyte was also purged with N_2 flow for about 30 min before the measurements. The applied potentials versus Hg/HgO ($E_{Hg/HgO}$) or Ag/AgCl ($E_{Ag/AgCl}$) RE were converted to the potentials versus RHE, E_{RHE}, using the Nernst equation as:

$$E_{RHE} = E_{Hg/HgO} + 0.059 \times pH + 0.098 \ (V) \quad (1)$$

$$E_{RHE} = E_{Ag/AgCl} + 0.059 \times pH + 0.222 \ (V) \quad (2)$$

where pH is the electrolyte pH. Applied ABPE is calculated using:[39]

$$ABPE\ (\%) = \frac{(J_{light} - J_{dark}) \times (1.23 - E_{RHE})}{P_{light}} \times 100\% \quad (3)$$

where J_{light} and J_{dark} are the measured current density (mA cm^{-2}) under illumination and at dark, respectively, at each biasing potential (Figure 3a), E_{RHE} is the applied potential (V) versus RHE, and P_{light} is the incident light power density (mW cm^{-2}) (which is 100 mW cm^{-2} here). A monochromator (Cornerstone 260) equipped with the solar simulator with the 1.5 AM filter as the light source was used to perform the spectral photoresponse and IPCE measurements. The monochromatic light spectrum was calibrated by a silicon photodiode (Newport 818-UV). Spectral photoresponse and IPCE measurements were carried out in the same three-electrode setup and electrolyte used for the current density measurements without using agitation and N_2 purging during the tests.

Supporting Information

Supporting Information is available from the Wiley Online Library or from the author.

© 2017 Wiley-VCH Verlag GmbH & Co. KGaA, Weinheim

Acknowledgements

This work was supported by the National Science Foundation (Grant No. NSF CBET1236155) and the Iwama Endowed Fund at UCSD. The TEM characterization performed at the University of Michigan was supported as part of the Center for Solar and Thermal Energy Conversion, an Energy Frontier Research Center funded by the U.S. Department of Energy, Office of Science, Office of Basic Energy Sciences under Award Number DE-SC0000957. A.K. thanks Dr. Bernd Fruhberger and cleanroom staff of UCSD Nano3 facilities for their support. A.K. acknowledges Dr. Conor T. Riley (UCSD) for his assistance with the optical absorption measurement.

[1] M. Gratzel, *Nature* **2001**, *414*, 338.
[2] N. S. Lewis, D. G. Nocera, *Proc. Natl. Acad. Sci. USA* **2006**, *103*, 15729.
[3] H. B. Gray, *Nat. Chem.* **2009**, *1*, 7.
[4] M. G. Walter, E. L. Warren, J. R. McKone, S. W. Boettcher, Q. Mi, E. A. Santori, N. S. Lewis, *Chem. Rev.* **2010**, *110* , 6446.
[5] D. Kim, K. K. Sakimoto, D. Hong, P. Yang, *Angew. Chem. Int. Ed.* **2015**, *54*, 3259.
[6] S. Y. Reece, J. A. Hamel, K. Sung, T. D. Jarvi, A. J. Esswein, J. J. H. Pijpers, D. G. Nocera, *Science* **2011**, *334*, 645.
[7] J. Luo, J.-H. Im, M. T. Mayer, M. Schreier, M. K. Nazeeruddin, N.-G. Park, S. D. Tilley, H. J. Fan, M. Grätzel, *Science* **2014**, *345*, 1593.
[8] M. Gong, W. Zhou, M. J. Kenney, R. Kapusta, S. Cowley, Y. Wu, B. Lu, M.-C. Lin, D.-Y. Wang, J. Yang, B.-J. Hwang, H. Dai, *Angew. Chem. Int. Ed.* **2015**, *127*, 12157.
[9] E. Verlage, S. Hu, R. Liu, R. J. R. Jones, K. Sun, C. Xiang, N. S. Lewis, H. A. Atwater, *Energy Environ. Sci.* **2015**, *8*, 3166.
[10] S. Hu, C. Xiang, S. Haussener, A. D. Berger, N. S. Lewis, *Energy Environ. Sci.* **2013**, *6*, 2984.
[11] C. Liu, J. Tang, H. M. Chen, B. Liu, P. Yang, *Nano Lett.* **2013**, *13*, 2989.
[12] P. Bornoz, F. F. Abdi, S. D. Tilley, B. Dam, R. van de Krol, M. Graetzel, K. Sivula, *J. Phys. Chem. C* **2014**, *118*, 16959.
[13] J.-W. Jang, C. Du, Y. Ye, Y. Lin, X. Yao, J. Thorne, E. Liu, G. McMahon, J. Zhu, A. Javey, J. Guo, D. Wang, *Nat. Commun.* **2015**, *6*, 7447.
[14] A. Kargar, J. Khamwannah, C.-H. Liu, N. Park, D. Wang, S. A. Dayeh, S. Jin, *Nano Energy* **2016**, *19*, 289.
[15] K. Zhang, M. Ma, P. Li, D. H. Wang, J. H. Park, *Adv. Energy Mater.* **2016**, *6*, 1600602.
[16] S. Hu, M. R. Shaner, J. A. Beardslee, M. Lichterman, B. S. Brunschwig, N. S. Lewis, *Science* **2014**, *344*, 1005.
[17] K. Sun, Y. Kuang, E. Verlage, B. S. Brunschwig, C. W. Tu, N. S. Lewis, *Adv. Energy Mater.* **2015**, *5*, 1402276.
[18] K. Sun, R. Liu, Y. Chen, E. Verlage, N. S. Lewis, C. Xiang, *Adv. Energy Mater.* **2016**, *6*, 1600379.
[19] F. Yang, A. C. Nielander, R. L. Grimm, N. S. Lewis, *J. Phys. Chem. C* **2016**, *120*, 6989.
[20] M. J. Price, S. Maldonado, *J. Phys. Chem. C* **2009**, *113*, 11988.
[21] C. Zhu, M. Zheng, Z. Xiong, H. Li, W. Shen, *Int. J. Hydrogen Energy* **2014**, *39*, 10861.
[22] T. Masaharu, N. Makoto, K. Akinobu, *Jpn. J. Appl. Phys.* **1969**, *8*, 358.
[23] I. J. Fritz, L. R. Dawson, G. C. Osbourn, *J. Electron. Mater.* **1985**, *14*, 73.
[24] I.-H. Tan, D. A. Vanderwater, J.-W. Huang, G. E. Hofler, F. A. Kish, E. I. Chen, T. D. Ostentowski, *J. Electron. Mater.* **2000**, *29*, 188.
[25] W. O. Groves, A. S. Epstein, *Google Patents*: *US 3931631 A*, **1976**.
[26] J. Sun, C. Liu, P. Yang, *J. Am. Chem. Soc.* **2011**, *133*, 19306.
[27] C. Liu, J. Sun, J. Tang, P. Yang, *Nano Lett.* **2012**, *12*, 5407.
[28] M. Malizia, B. Seger, I. Chorkendorff, P. C. K. Vesborg, *J. Mater. Chem. A* **2014**, *2*, 6847.
[29] A. J. Nozik, *Appl. Phys. Lett.* **1976**, *29*, 150.
[30] K. Ohashi, J. McCann, J. O. M. Bockris, *Nature* **1977**, *266*, 610.
[31] B. Kaiser, D. Fertig, J. Ziegler, J. Klett, S. Hoch, W. Jaegermann, *ChemPhysChem* **2012**, *13*, 3053.
[32] A. Standing, S. Assali, L. Gao, M. A. Verheijen, D. van Dam, Y. Cui, P. H. L. Notten, J. E. M. Haverkort, E. P. A. M. Bakkers, *Nat. Commun.* **2015**, *6*, 7824.
[33] V. K. Subashiev, G. A. Chalikyan, *Phys. Status Solidi B* **1966**, *13*, K91.
[34] S. Sukrittanon, R. Liu, Y. G. Ro, J. L. Pan, K. L. Jungjohann, C. W. Tu, S. A. Dayeh, *Appl. Phys. Lett.* **2015**, *107*, 153901.
[35] G. Y. Rudko, I. A. Buyanova, W. M. Chen, H. P. Xin, C. W. Tu, *Solid-State Electron.* **2003**, *47*, 493.
[36] S. W. Boettcher, E. L. Warren, M. C. Putnam, E. A. Santori, D. Turner-Evans, M. D. Kelzenberg, M. G. Walter, J. R. McKone, B. S. Brunschwig, H. A. Atwater, N. S. Lewis, *J. Am. Chem. Soc.* **2011**, *133*, 1216.
[37] V. Narayanan, S. Mahajan, K. J. Bachmann, V. Woods, N. Dietz, *Philos. Mag. A* **2002**, *82*, 685.
[38] J. Zhu, C.-M. Hsu, Z. Yu, S. Fan, Y. Cui, *Nano Lett.* **2010**, *10*, 1979.
[39] Z. Chen, H. Dinh, E. Miller, *Photoelectrochemical Water Splitting Standards, Experimental Methods, and Protocols*, Springer-Verlag, New York, USA **2013**.

Received: October 25, 2016
Revised: January 25, 2017
Published online: March 31, 2017

© 2017 Wiley-VCH Verlag GmbH & Co. KGaA, Weinheim